Summary of Results from the Telescope Array Experiment

Charles C. H. Jui[*]

Department of Physics and Astronomy, University of Utah
E-mail: jui@physics.utah.edu

for the Telescope Array Collaboration [†]

The Telescope Array (TA) is the largest experiment in the northern hemisphere actively observing ultrahigh energy cosmic rays. TA is a hybrid detector system combining the precision of the air fluorescence technique with the efficiency of a surface scintillator array. Three fluorescence stations each view $108°$ in azimuth and up to $30°$ in elevation. They are located at the periphery of a ground array consisting of 507 plastic scintillator counters. The surface detectors are arranged in a square grid of 1.2km spacing, covering over 700 square kilometers. TA has now collected over seven years of data. We present the cosmic ray spectra from both TA and its low energy extension (TALE), covering a range of energies from below 10^{16} eV to over 10^{20} EeV. We also discuss the latest results from the measurements of mass composition by the TA group. Finally, we present our results from the search for arrival direction anisotropy, including the observed large excess of events at the highest energies, seen in the region of the northern sky centered on Ursa Major. Based on the current results, TA is vigorously pursuing expansion of our detectors to four times its current size.

---

[*]Speaker.

[†]Full author list and Acknowledgements: http://www.telescopearray.org/images/papers/ICRC2015-authorlist.pdf

1. introduction

The Telescope Array experiment is located in the West Desert of Utah, near the town of Delta. The TA detector has been in operation since 2008. It consists of 507 surface detectors (SD) arranged in a square grid of 1.20 km spacing. A total of 38 telescopes are distributed among three fluorescence detector (FD) stations at the periphery of the array marked (Black Rock, Long Ridge, and Middle Drum). These look inward and observe the airspace above the surface detectors. The layout of the TA experiment is shown in Figure 1. The TA collaboration is an international group with member institutions from Japan, U.S., South Korea, Russia, and Belgium.
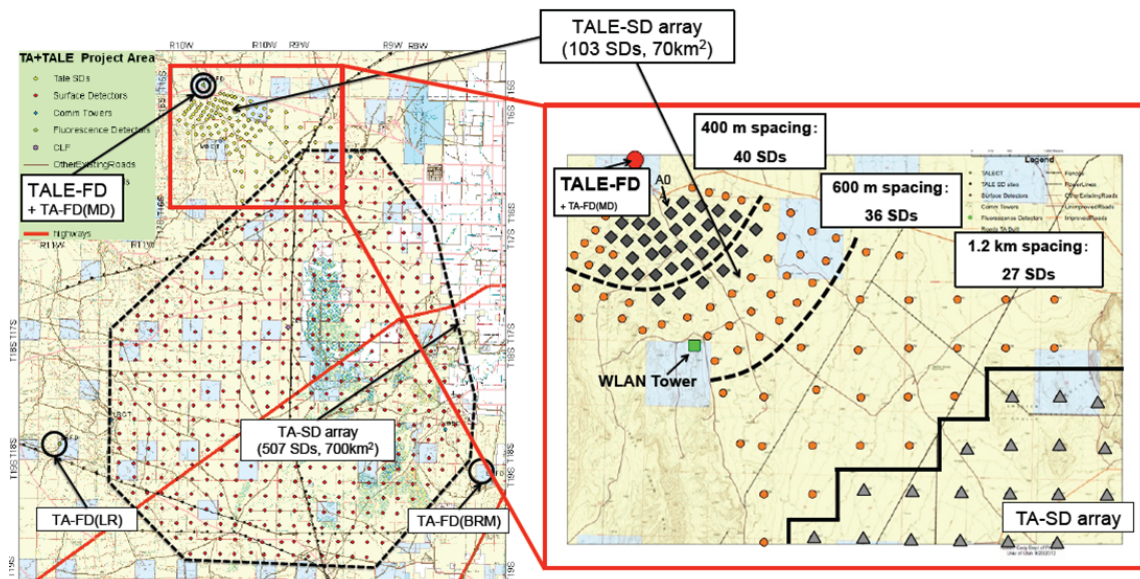

Figure 1: Layout of the Telescope Array detector site. The main array is shown on the left with a surface detector (SD) array of 507 scintillation counters surrounded by three fluorescence detector (FD) stations (MD: Middle Drum, BRM: Black Rock mesa, LR: Long Ridge) looking inward over the SD. The expanded inset on the right shows the layout of the TA Low-energy Extension (TALE). TALE consists of 10 new high-elevation $(31° − 59°)$ fluorescence telescopes located at the MD site, and an in-fill SD array of 103 counters arranged with spacings that grows with distance from the TALE FD, in order to make optimal coverage at energies below 10^{18} eV.

In addition to the main TA SD array and FD stations, a new TA Low-energy Extensions (TALE) is under construction. the first stage of ten high-elevation FD telescopes (TALE FD) are complete, and about one year of data has already been taken. An accompanying in-fill SD array with graded spacing is also under construction, with 32 of the 103 units already in place, and 16 counters now in operation. The expanded inset of Figure 1 shows the layout of the TALE FD and SD array.

In this highlight presentation, we discuss the latest results from TA in the measurements of spectrum of cosmic ray spectrum at the highest energies, their composition, as well as anisotropies in their arrival directions. These were distributed over a number of contributed presentations during the 34th ICRC. The TA results give a consistent picture of a single light component of extragalactic origin, leading to the observation of the expected GZK cut-off in the energy spectrum.

The observation of a hotspot in the arrival directions suggests the possibility of a local source or sources.

2. Energy Spectrum

TA had previously published an energy spectrum from the first four years of SD operation [1]. At the 2015 ICRC, TA presented a new combined spectrum that spans in energy from below 10^{16} eV to just above 10^{20} eV, shown in Figure 2. This plot combines the SD spectrum (upright triangles) from seven years of operation [2], the monocular FD spectrum (inverted triangles) [3], and the TALE fluorescence spectrum (open circles) [4]. In addition, the spectrum obtained by a newly developed technique of monocular reconstruction of events dominated by Čerenkov light is also included [5].
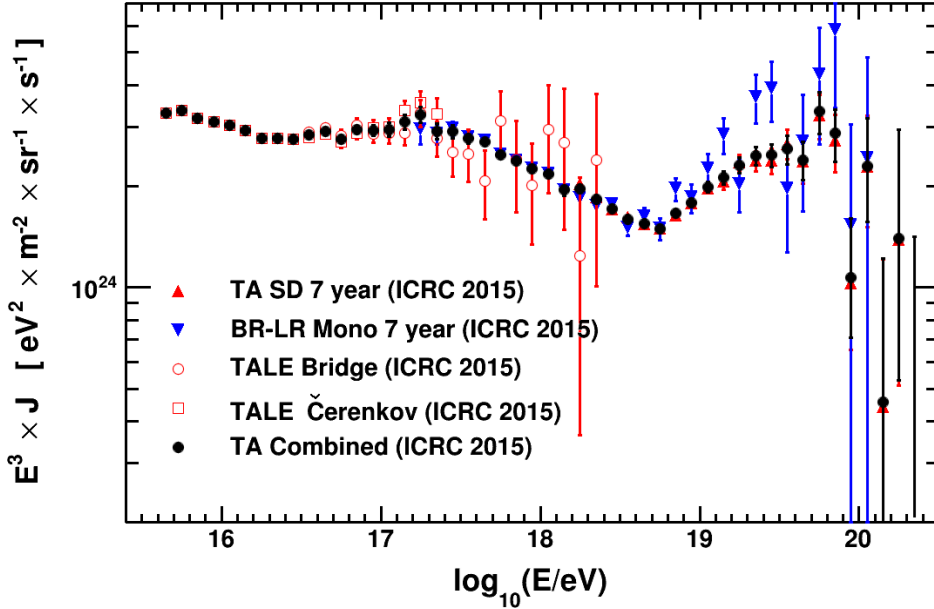

Figure 2: Combined spectrum from the Telescope Array Collaboration, including the 7 year surface detector spectrum (upright triangles), the 7 year monocular spectrum from the Black Rock and Long Ridge fluorescence detectors (inverted triangles), the TALE fluorescence spectrum (open circles), and the TALE Čerenkov spectrum (open squares). The averaged spectrum combining these four measurements is shown by the black circles.

The SD spectrum shows a GZK cut-off [6, 7] at 6σ significance with a break in the spectrum at $log(E/\mathrm{eV}) = 19.78 \pm 0.06$. A *dip* or *ankle* structure is also seen at $log(E/\mathrm{eV}) = 18.70 \pm 0.02$. The simplest explanation for the combination of spectral features is that of interaction between extragalactic cosmic ray protons and the cosmic microwave background radiation (CMBR) attenuating the flux via photo-pion production above the cut-off, and by e^+e^- pair production above the ankle [8]. The TA spectrum shows an apparent break at just above 10^{17} eV consistent with the "Second Knee" feature [9]. Another *dip* feature is seen just above the 10^{16} eV, which has been reported by other experiments [10, 11].

The part of the TA SD spectrum above $10^{18.2}$ eV has also been fitted to an extra-galactic source distance distribution parameterized by the function $(1+z)^m$, where z is the red-shift, and m the evolution parameter. A pure flux of protons is assumed with a power-law injection spectrum of the form E^{-p}. The results are summarized in Figure 3 [12], where plot (a) shows the best-fit curve overlaid on the measured flux, and plot (b) shows the confidence contours. The best fit values are $p = 2.18^{+0.08}_{-0.14}$, and $m = 6.8^{+1.6}_{-1.1}$ (uncertainties include both statistical and systematic contributions). While the evolution parameter is relatively large, there is considerable (anti-)correlation between the two parameters. In any case, Figure 3(b) shows good agreement between the fit and data in the region of the GZK cut-off from purely protons. As was suggested during the contributed sessions, we plan to make this fit for compositions other than proton, as a completely orthogonal measure of composition of the highest energy cosmic rays, to that given by X_{MAX} measurements.
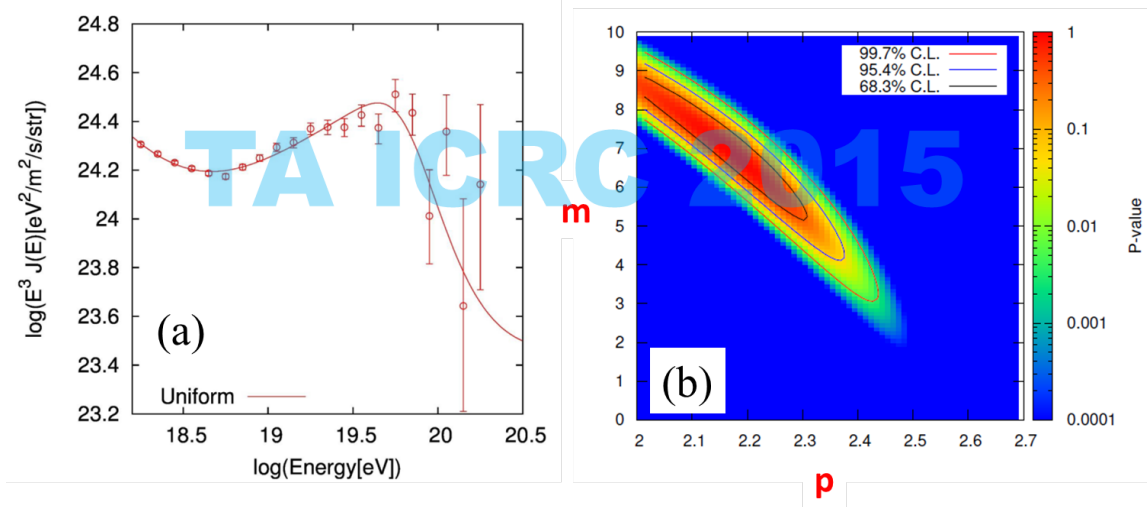

Figure 3: Results of a fit of the TA cosmic ray energy spectrum above $10^{18.2}$ eV to a source distribution parameterized by the function $(1+z)^m$, where z is the red-shift, and m the evolution parameter. A pure protonic flux is assumed with a power-law injection spectrum of the form E^{-p}.

3. Composition Results using X_{MAX}

The standard measurement of ultrahigh energy cosmic ray composition has been that of the shower maximum depth, X_{MAX}. TA has already published the result from four years of hybrid events collected from the TA Middle Drum FD in coincidence with the surface array [13]. When compared to QGSJET-II.3, the results showed a predominately light composition consistent with protons. Figure 4 shows the updated plot of mean X_{MAX} vs $logE$ from this measurement with now seven years of data [14]. A measurement of mean X_{MAX} vs. $logE$ from hybrid events from the Black Rock and Long Ridge FD is also shown in Figure 5 [15].

As a complement to the hybrid measurements, TA also made a measurement of X_{MAX} using stereoscopic events seen in coincidence between the Long Ridge and Black Rock FD stations [16]. The average X_{MAX} vs. $logE$ plot from this study is shown in Figure 5. The summary of TA X_{MAX} measurements is shown in Figure 7(a), where we plot the position of the measured points from
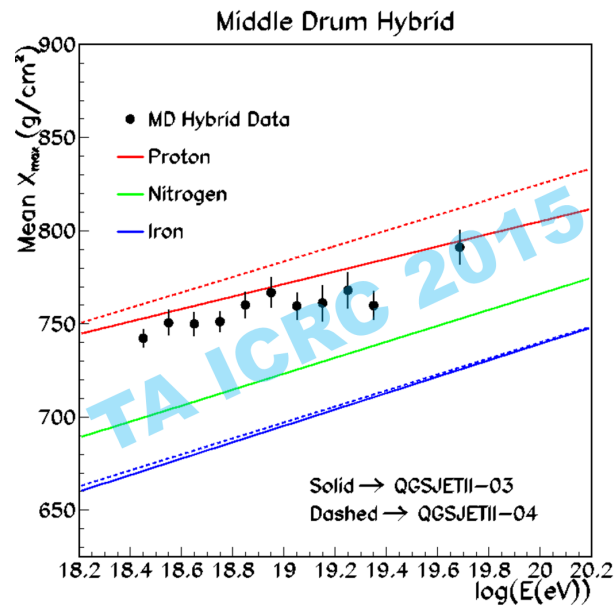
Figure 4: Average X_{MAX} vs. energy for hybrid events collected between 2008 and 2015 from the Middle Drum FD station, in coincidence with the TA surface array.
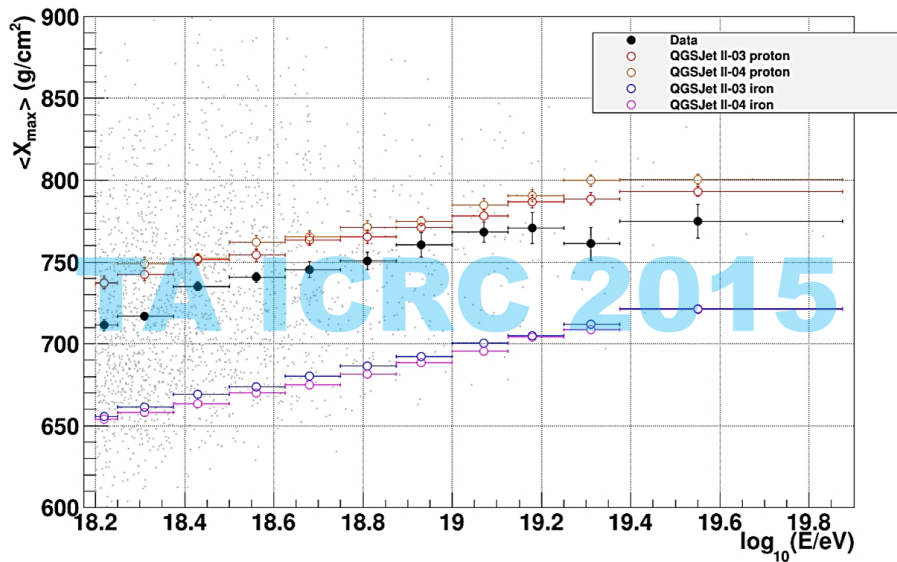

Figure 5: Average X_{MAX} vs. energy for hybrid events collected from the Black rock and Long Ridge FD stations, in coincidence with the TA surface array.

the three studies relative to the simulated proton (1.0) and iron (0.0) rails obtained from showers simulated using the QGSJET-II.3 hadronic model [17].
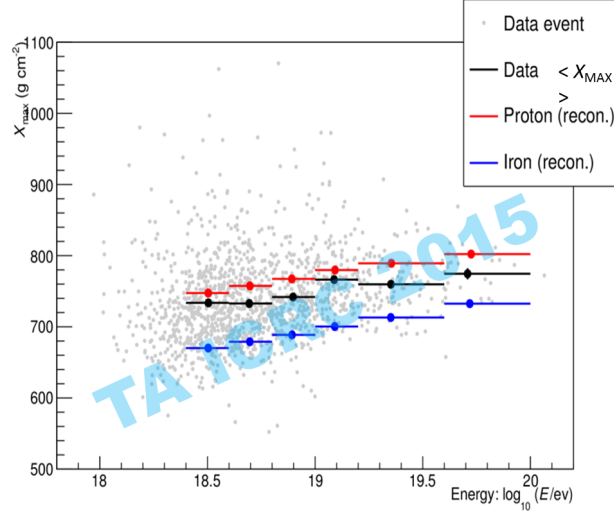

Figure 6: Average X_{MAX} vs energy for stereo events observed in coincidence between the Black Rock and Long Ridge FD stations.

The three sets of data points are in good agreement with one another as well as a predominately light composition. While the rails used to make Figure 7(a) are based on QGSJET-II.3, the interpretation of light composition is fairly robust, as illustrated by the scales shown in Figure 7(b). To leading order, the departure of the data points from the proton line is roughly proportional to lnA where A is the nuclear mass number. Even if the scale were set to a hypothetical model that has a proton rail that is 33% deeper, the data points shown in the plot would only reach that expected for helium in this scenario.

TA has recently published a measurement of the inelastic proton-air cross section [18], using the hybrid FD data set from the Middle Drum station. The results are summarized in Figure 8 [19]. The deep tail of the measured X_{MAX} distribution is fitted to an exponential function in Figure 8(a), yielding a best-fit (negative) exponent of $\Lambda = 50.47 \pm 6.26$ [stat.] g/cm^2, which translates to a result of $\sigma_{p-air}(inelastic) = 567.0 \pm 70.5$ [Stat.] $(+25, -29)$ [Sys.] mb. The dominant contributions to the systematic uncertainty come from model dependence of the Λ exponent in relation to the cross section, and from the possible presence of ultrahigh energy photons and helium affecting the tail of the X_{MAX} distribution. This TA value for the proton-air cross-section appears to be consistent with the trend seen from previous results, as illustrated in Figure 8(b)

4. Anisotropy

After five years of operations, a hotspot was seen in the arrival direction of TA SD events of energies above 5.7×10^{19} eV. This was described in a publication in 2014 [20]. Of the 72 events above this threshold, shown by the blue points in Figure 9, 19 were found within 20° of right ascension(α)= 146.7° and declination(δ)= 43.2°, in the vicinity of Ursa Major. The red points in the figure show the events collected in the two additional years of data [21]. Four more events
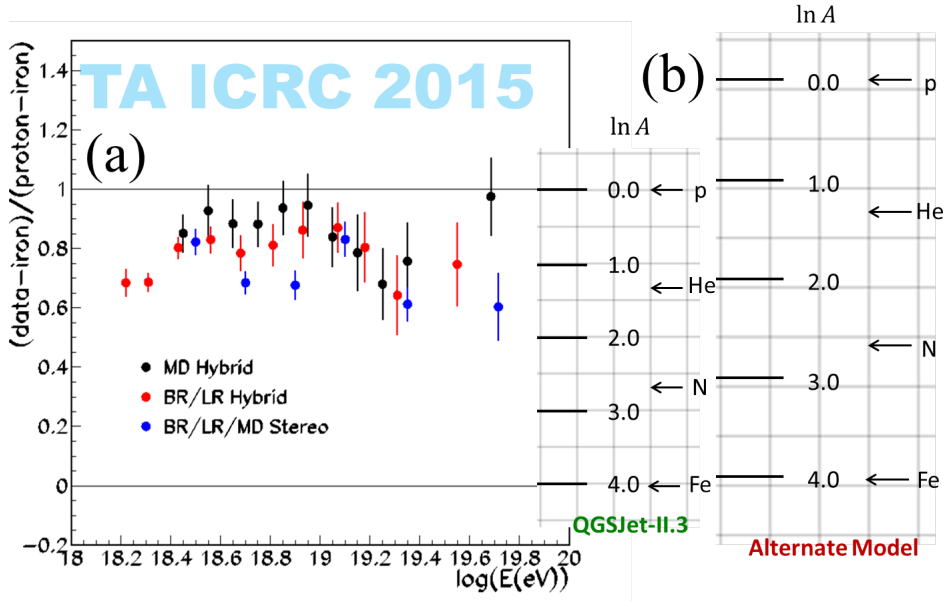
Figure 7: (a) Summary of average X_{MAX} from Telescope Array fractional as the fractional position between the expectations of pure iron (lower lines at zero) and pure proton (upper line at 1.0) using the QGSJET-II.3 hadronic model. (b) Illustrative interpretation, in terms of *lnA* of the summary plot against QGSJET-II.3 and a hypothetical alternative model where the proton rail is about 33% deeper in X_{MAX}.

(three in the sixth, and one in the seventh) were seen inside the original 20° circle. With the full seven years of data, the maximum moved slightly to RA= 148.5° and dec= 44.6°, but now with a total of 24 events (still 3 and 1 from years 6 and 7, respectively) within 20° of this location.

The maximum Li-Ma significance corresponding to excess after seven years is 5.1σ, as shown in Figure 10 [21]. To assess the global significance of this hotspot, one million simulated sets of exactly 109 events were generated assuming an isotropic source distribution. We searched for an excess anywhere in the FOV with five radii, 15°, 20°, 25°, 30°, and 35°. From these, the chance probability of seeing a maximum local excess somewhere in the TA field-of-view was calculated to be 3.7×10^{-4}, corresponding to a global significance of 3.4σ.

It has been noted that the number of events in the signal circle occurred at a lower rate in the sixth and seventh year. The chance probability of observing four or fewer events in the signal circle over two years given the original 19 over five years is about 20%. Moreover, the histogram shown in Figure 11(a) indicates that the observed distribution of number of signal events per year is completely consistent with that of a Poisson distribution with a mean of 3.43. The comparison of the cumulative distribution in Figure 11(b) [21] also shows the observed distribution to be incompatible with an isotropic background distribution (blue dotted curve: mean = 0.9) at the 2.6σ level.

It is important to note that the hotspot is only found for events in the energy range at and above the GZK cut-off, but not with lower energy thresholds of 1.0×10^{19} eV or 4.0×10^{19} eV. The hotspot also appears with an angular size of the order of 10°. Our observations are consistent with the hypothesis of an extra-galactic flux of protons coming from a single source, or a compact group of sources within the GZK horizon of about 100 Mpc. In this picture the CMBR interactions
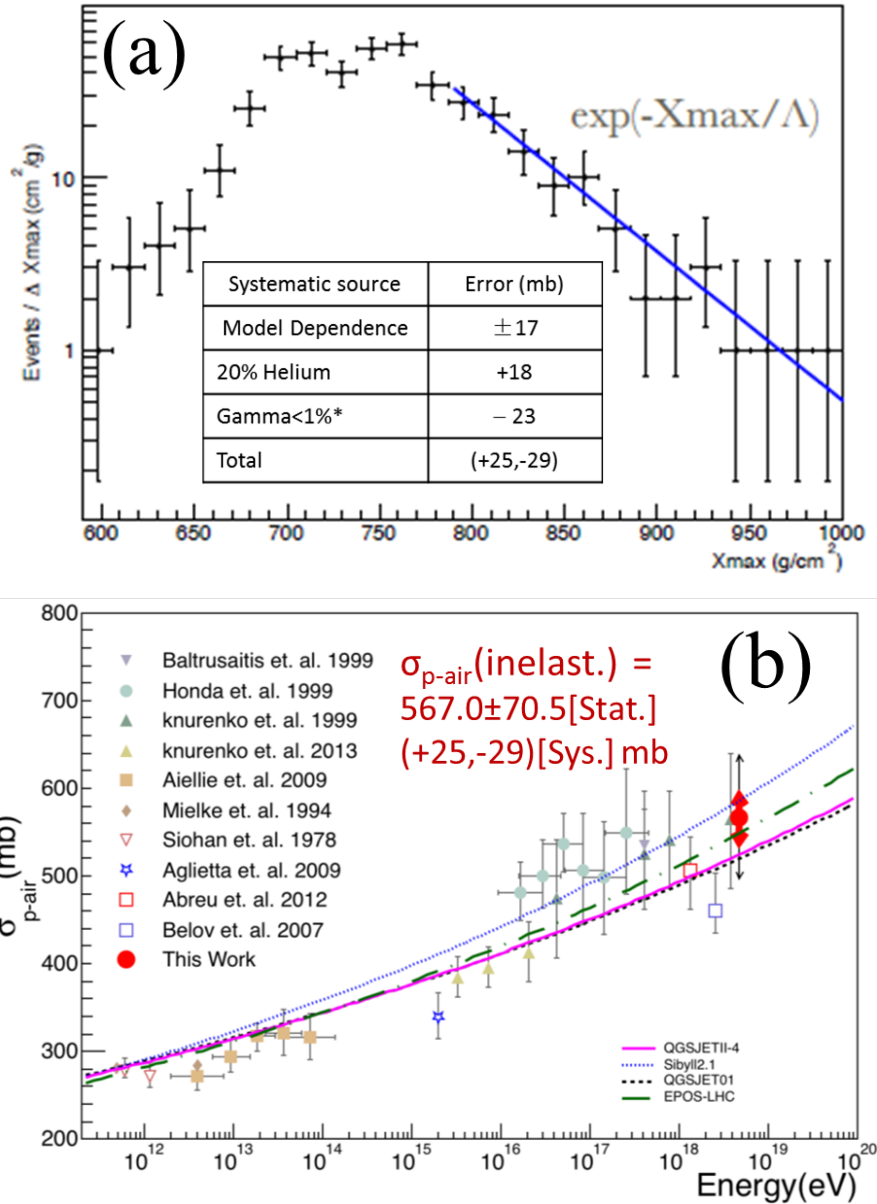
Figure 8: Plot (a) shows the fit of the tail of the X_{MAX} distribution from the TA Middle Drum hybrid FD events data to an exponential function. The resulting slope is used to calculate the inelastic proton-air collision cross-section. The TA result is shown in plot (b) along with those of previous experiments [19].
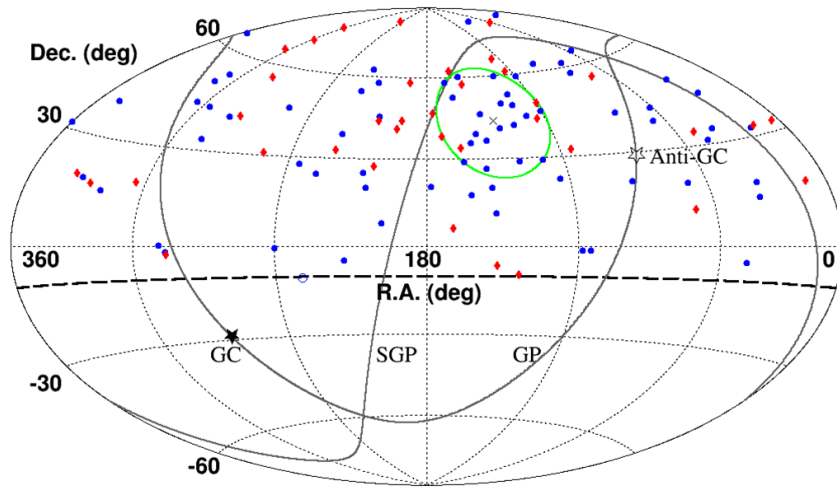
Figure 9: Arrival directions, plotted in equatorial coordinates, of TA events with energies above 5.7×10^{19} eV. The blue points represent the 72 events collected in the first five years of operation [20]. The red points represent 37 additional events collected over two additional years [21]. The solid curves indicate the galactic plane (GP) and Super-Galactic Plane (SGP), and the closed and open stars indicate the Galactic center (GC) and the anti-Galactic center (Anti-GC), respectively
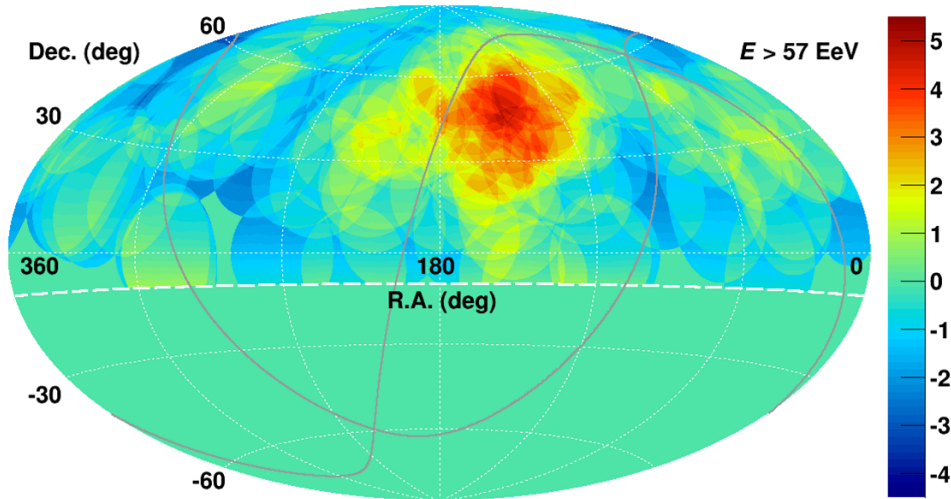
Figure 10: Li-Ma excess significance (number of σ) of local excess in number of events above expected isotropic background within $20°$ of each spot in the field-of-view of TA for data collected between 2008 and 2015. The solid curves indicate the galactic plane (GP) and Super-Galactic Plane (SGP).
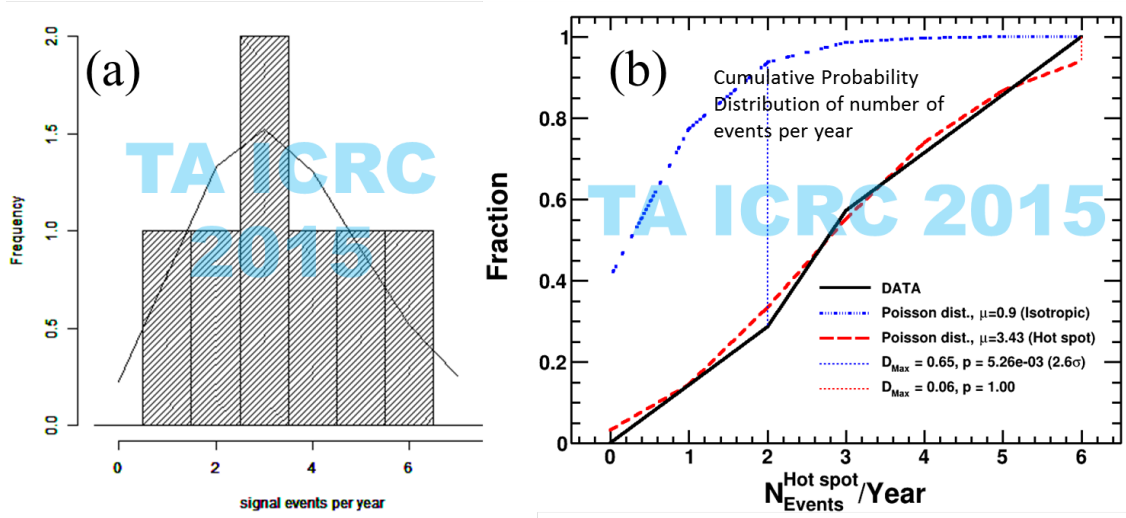
Figure 11: (a) Distribution of number of events within $20°$ of (RA, dec) = $(148.5°, 44.6°)$. The solid line shows the expectation of a Poisson distribution with a mean of 3.43. (b) A comparison of the cumulative distribution of number of signal events per year with the prediction (black line) with the expectations for a Poisson distribution (red dashed curve) and an isotropic background distribution with a mean of 0.9. From the maximum deviations the Kolmogorov-Smirnov probabilities for the source model is 1.0, and that for the isotropic model is 5.26×10^{-3} [21]. The latter corresponds to a 2.6σ deviation.

would filter out the background events from more distant sources for energies at or above the GZK cut-off, leaving the image of a local source distribution smeared by magnetic fields.

There are additional indications of departure from isotropy in the highest energy data set ($> 5.7 \times 10^{19}$ eV) [22, 23]. Figure 12 shows the result of a search for autocorrelation in the arrival direction of events with thresholds of $1.0\times$, $4.0\times$, and 5.7×10^{19} eV [23]. The probability of random excesses from isotropic distributions for different separation angles between pairs of events are calculated for the actual data. It is clear that a significant excess is seen only for the highest energy threshold, with a minimum p value of less than 10^{-3} at an angular scale of about $25°$.

Significant departures from isotropy are also seen in the histogram of events in plotted in right-ascension(RA)/declination(dec) or in supergalactic longitude/latitude [23]. Figure 13 shows excesses at about the 2σ level in all four variable. The data in blue are compared with a simulation of isotropic source distributions in red, using the Kolmogorov-Smirnov test for compatibility. The resulting p values again depart from isotropy at about the 2σ level. Similar comparisons at lower energy thresholds showed no significant departures from isotropy.

It is interesting to note that the bin excesses in Figure 13 appear most significant in the super-galactic latitude. This observation suggests the possibility that the excess may be correlated with the local large-scale structure (LSS) of galaxies, which are concentrated around the Super-Galactic Plane (SGP). The hotspot shown in Figure 10 also lies close to the SG plane.

A more direct test of this hypothesis was made using the TA SD data [22, 23]. Using the 2MASS Red Shift Catalog, we simulated the arrival directions of cosmic ray protons with $E > 5.7 \times 10^{19}$ eV, accounting for flux attenuation from propagation through the cosmic microwave background radiation, and where stochastic effects of magnetic deflection is simulated using angu-
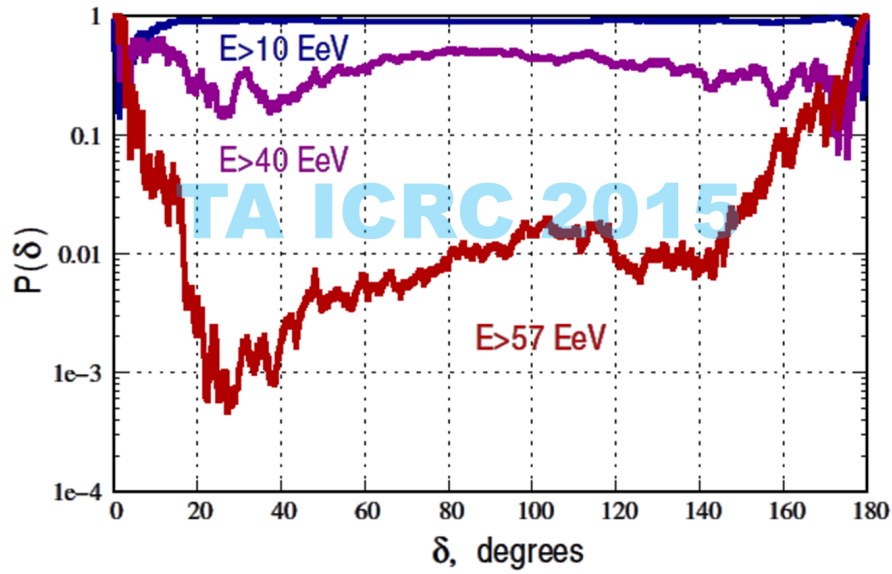
10

Figure 12: Probability of random excess of pairs of TA events (seven years) vs. separation angle δ at energies above $1.0\times$, $4.0\times$, and 5.7×10^{19} eV.
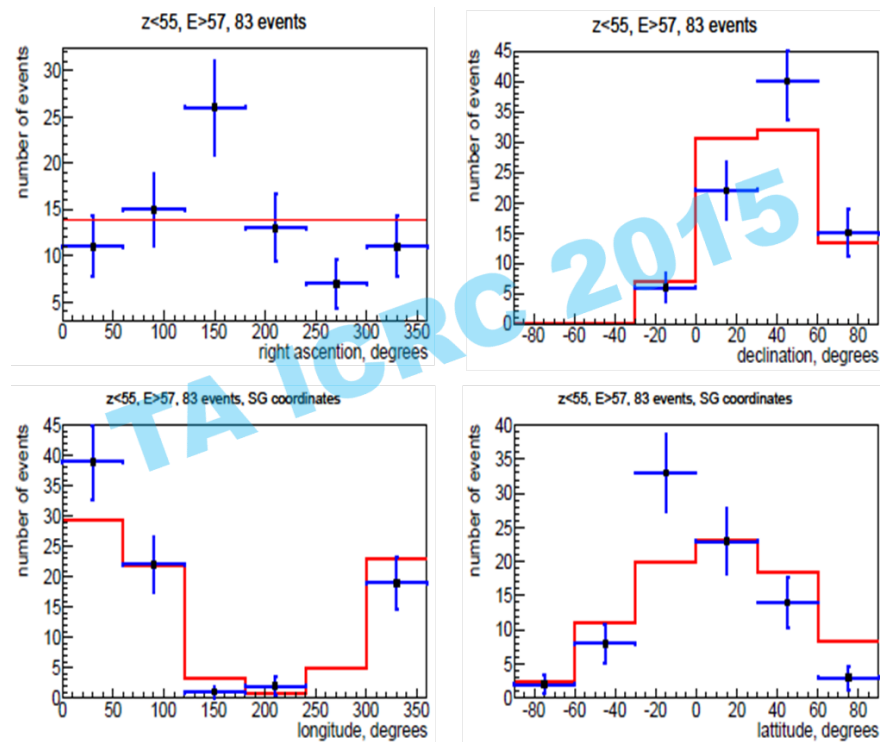

Figure 13: Histograms of TA SD events recorded from 2008 to 2014 in Right-Ascension (top-left), declination (top-right), supergalactic longitude (bottom-left) and latitude (bottom-right). The data are shown in blue points overlaid with isotropic simulations. The Kolmogorov-Smirnov probabilities comparing data with simulation are shown with each plot.

11

lar smearing. The final distribution is also convolved with detector exposure over the data collection period. An example of such a density distribution generated using a smearing angular scale of 6° is shown in Figure 14, where the white dots show the arrival directions of the TA SD events collected from 2008 to 2015 previously shown in Figure 9.
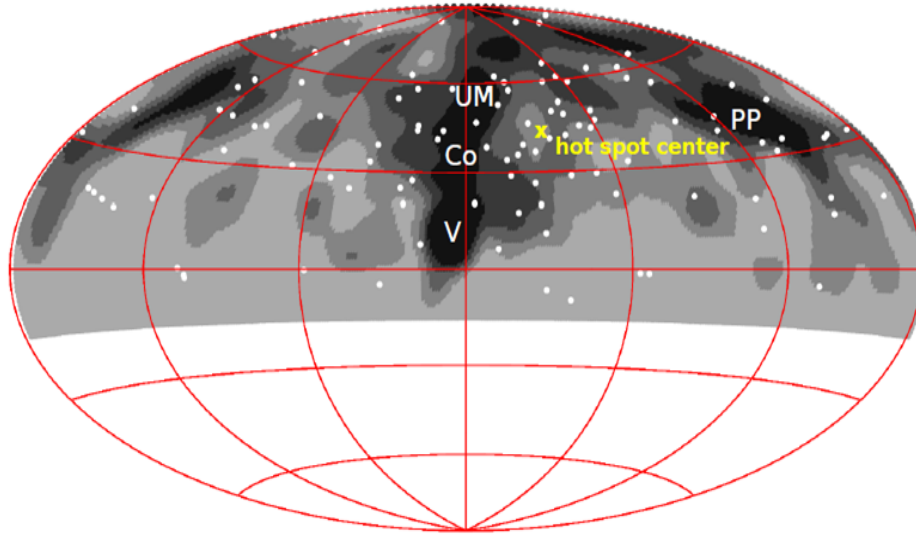
Figure 14: (a) Density of expected arrival distribution for events above 5.7×10^{19} eV. The simulation assumed cosmic ray protons that originate uniformly from the local distribution of matter (2MASS Galaxy Red Shift Catalog). A smearing angle of 6° is used in this map. UM–Ursa Major; Co–Coma; V–Virgo; PP–Perseus-Pisces.

Density distribution were generated from both the LSS model and an isotropic model for threshold energies of $1.0\times$, $4.0\times$, and 5.7×10^{19} eV, each repeated for smearing angles between 2° and 31° in 1° increment. Using the Kolmogorov-Smirnov test, the distribution of density values from arrival directions of data events is compared to those obtained from these simulations. For the two lower energy thresholds, the data cannot distinguish between the LSS structure and isotropy. However, at above 5.7×10^{19} eV, the LSS model is clearly preferred for smearing angles greater than 5°, as shown in Figure 15.

5. Summary

TA has measured the energy spectrum, composition and arrival direction of UHE cosmic rays since 2008. The energy spectrum and composition of UHE cosmic rays measured by TA are compatible with a single light component at above the ankle (6×10^{18} eV). The new TA Low Energy Extension (TALE) is now coming on line, and has already extended the TA energy spectrum to below 10^{16} eV. We have reported a hot spot seen in the direction of Ursa Major with 3.4σ significance, but much more data is needed. This find has prompted TA to propose a major upgrade that will expand the coverage area of TA to four times that of the existing array (TA$\times$4) [24]. Funding for the additional surface detectors has already been funded by the government of Japan, and the U.S. part of the TA collaboration has submitted a proposal to augment the fluorescence detectors
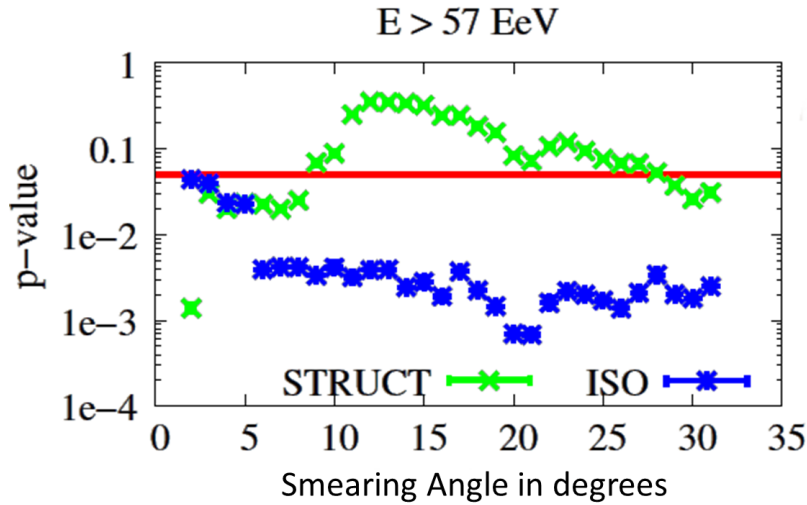
Figure 15: Kolmogorov-Smirnov *p*-values plotted against smearing angle for TA data 5.7×10^{19} eV collected from 2008 to 2015 compared against the density distributions generated from LSS source model (green "X" marks) vs. that for an isotropic source model (blue asterisks). The LSS model is preferred over that of the isotropic for smearing angles larger than about $5°$

to cover all of the new surface array. By 2020, we will have collected the equivalent of about 20 years of TA data.

Acknowledgments

References

[1] T. Abu-Zayyad et al. (TA Collaboration), Astrophys. Journal Letters **768**, L1 (2013).

[2] D. Ivanov for the TA Collaboration, in proceedings of *the 34th ICRC*, `Pos(ICRC2015)349` (2015).

[3] T. Fujii for the TA Collaboration, in proceedings of *the 34th ICRC*, `Pos(ICRC2015)320` (2015).

[4] Z. Zundel for the TA Collaboration, in proceedings of *the 34th ICRC*, `Pos(ICRC2015)445` (2015).

[5] T. Abu-Zayyad for the TA Collaboration, in proceedings of *the 34th ICRC*, `Pos(ICRC2015)422` (2015).

[6] K. Greisen, Phys. Rev. Lett. **16**, 222 (1966).

[7] G.T. Zatsepin and V.A. Kuz'min, JETPL **4**, 78 (1966).

[8] V. Berezinsky, A.Z. Gazizov, and S.I. Grigorieva, Physics Letters B **612**, 147 (2005).

[9] D.R. Bergman and J.W. Belz, J.Phys. **G34**, R359 (2007).

[10] W.D. Apel *et al.* (KASCADE-Grande Collaboration) Astropart. Phys. **36**, 183 (2012).

[11] M.G. Aartsen *et al.* (IceCube Collaboration) Phys. Rev. D **88**, 042004 (2013).

[12] E. kido for the TA Collaboration, in proceedings of *the 34th ICRC*, `Pos(ICRC2015)258` (2015).

[13] R.U. Abbasi *et al.* (TA Collaboration), Astropart. Phys. **64**, 49 (2015).

[14] J.P. Lundquist for the TA Collaboration, in proceedings of *the 34th ICRC*, `Pos(ICRC2015)441` (2015).

[15] D. Ikeda, W. Hanlon for the TA Collaboration, in proceedings of *the 34th ICRC*, `Pos(ICRC2015)362` (2015).

[16] T. Strohman and Y. Tameda for the TA Collaboration, in proceedings of *the 34th ICRC*, `Pos(ICRC2015)361` (2015)

[17] J.W. Belz for the TA Collaboration, in proceedings of *the 34th ICRC*, `Pos(ICRC2015)351` (2015).

[18] R.U. Abbasi *et al.* (TA Collaboration), Phys. Rev. D **92**, 032007 (2015).

[19] R.U. Abbasi and J.W. Belz for the TA Collaboration, in proceedings of *the 34th ICRC*, `Pos(ICRC2015)402` (2015).

[20] R.U. Abbasi *et al.* (TA Collaboration), Astrophysical Journal Letters **790**, L21 (2014).

[21] K. Kawata for the TA Collaboration, in proceedings of *the 34th ICRC*, `Pos(ICRC2015)276` (2015).

[22] T. Abu-Zayyad *et al.* (TA Collaboration), Astrophysical Journal **777**, 88 (2013).

[23] P. Tinyakov, H. Sagawa, and I. Tkachev for the TA Collaboration, in proceedings of *the 34th ICRC*, `Pos(ICRC2015)326` (2015).

[24] H. Sagawa for the TA Collaboration, in proceedings of *the 34th ICRC*, `Pos(ICRC2015)657` (2015).